The 4th European sCO_2 Conference for Energy Systems
March 23-24, 2021, Online Conference

2021-sCO2.eu-101

SIMULATION AND ANALYSIS OF A SELF-PROPELLING HEAT REMOVAL SYSTEM USING SUPERCRITICAL CO_2 AT DIFFERENT AMBIENT TEMPERATURES

Markus Hofer*
University of Stuttgart
Stuttgart, Germany
Email: hofer@ike.uni-stuttgart.de

Haikun Ren
University Duisburg-Essen
Duisburg, Germany

Frieder Hecker
Simulator Centre of KSG | GfS
Essen, Germany

Michael Buck
University of Stuttgart
Stuttgart, Germany

Dieter Brillert
University Duisburg-Essen
Duisburg, Germany

Jörg Starflinger
University of Stuttgart
Stuttgart, Germany

ABSTRACT

Innovative heat removal systems are currently investigated for use in existing and future nuclear power plants. One of them is the supercritical carbon dioxide (sCO_2[1]) heat removal system, which is based on a closed Brayton cycle with sCO_2 as a working fluid.

This paper provides the design and layout of the sCO_2 cycle based on assumptions developed in the project sCO2-4-NPP. The system is analysed over a wide range of ambient and steam-side conditions in ATHLET, using performance maps for the turbomachinery, which were designed recently. Bypasses are considered in the layout of the cycle to cope with special operation conditions, e.g. start-up. Different operational readiness states for the system are shown, which enable a fast start-up of the system. Air mass flow rate control is implemented to keep the compressor inlet temperature constant with controller parameters depending on the ambient temperature.

The performance analysis of the system suggests that it is a good option to operate the system at the design compressor inlet temperature of 55 °C at any ambient or steam-side boundary condition. With decreasing thermal power input, the rotational speed of the turbomachinery must be decreased to keep the system self-propelling. Turbomachinery design with a higher surge margin is preferred and different operation strategies are feasible and need to be tested in interaction with the nuclear power plant.

INTRODUCTION

In case of a station blackout and loss of ultimate heat sink accident in a boiling water reactor or pressurized water reactor, the plant accident management strongly depends on the recovery of electricity, e.g. by emergency diesel generators, or from external sources. If not available, core integrity will be violated, like in Fukushima Dachii accident. Such scenarios inspire the development of advanced decay heat removal systems. Since space is a limitation in existing power plants, the supercritical carbon dioxide (sCO_2) heat removal system "sCO2-HeRo" was proposed because of its compactness and self-propelling features [1–3]. Such a system could be incorporated in newly-built nuclear power plants as well as retrofitted to existing nuclear power plants. The system consists of a compact heat exchanger (CHX), a gas cooler, serving as the ultimate heat sink (UHS), and the turbomachinery, one compressor and one turbine mounted on a common shaft together with a generator. Since the momentum from the turbine is sufficient to simultaneously drive the compressor and generate more electricity than used by the fans of the UHS, the system is self-propelling. The excess electricity can even be used to support other accident measures, e.g. recharging batteries. CO_2 is selected as a working fluid because of its favourable fluid properties, enabling the design of a very compact system. Moreover, CO_2 is not combustible, non-toxic and commercially available. Figure 1 shows the scheme of the sCO2-HeRo attached to the reactor pressure vessel of a boiling water reactor or to the steam generator of a pressurized water reactor. In the case of an accident in a boiling water reactor, the

[1] sCO_2 is defined as carbon dioxide at supercritical conditions with $p > 73.8$ bar and $T > 31$ °C

* corresponding author(s)

DOI: 10.17185/duepublico/73943

valve, which connects the CHX to the main steam line, opens automatically. Driven by natural circulation, the steam condenses and heats the sCO_2 in the CHX. The pressurized and heated sCO_2 is expanded in the turbine, which drives the compressor and generates power for the fans of UHS. After the turbine, the remaining heat of the sCO_2 is removed in the UHS. Finally, the sCO_2 is compressed and flows to the CHX. Similarly, the sCO2-HeRo can be attached to the secondary side of a pressurized water reactor. In the primary loop, natural circulation will develop due to the decay heat input from the reactor core and heat removal via the steam generator. Consequently, the sCO2-HeRo principle could be used for boiling water reactors as well as pressurized water reactors. Generally, it is important to analyse the interaction of the sCO2-HeRo system with the nuclear plant for both reactors separately due to their different thermal-hydraulic behaviour and restrictions. However, the sCO_2 loop should also be analysed separately to gain knowledge on the operation of the loop which can be used for both reactor types.

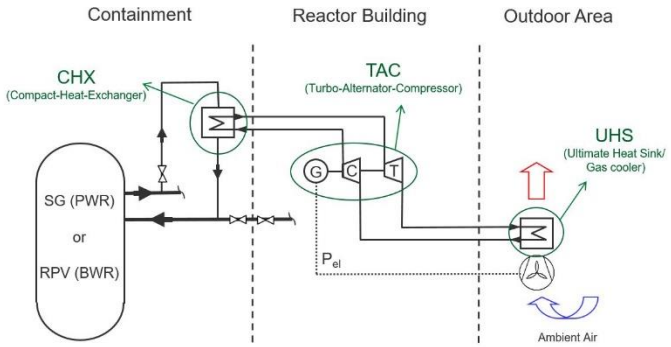

Figure 1: The sCO2 heat removal system attached to the reactor pressure vessel (RPV) of a boiling water reactor (BWR) [1] or to the steam generator (SG) of a pressurized water reactor (PWR)

For the simulation of the thermo-hydraulic behaviour of nuclear power plants, different system codes are used, e.g. CATHARE, RELAP, TRACE, ATHLET and SCTRAN [4,5]. Because sCO_2 is considered as a working fluid for 4th generation reactor concepts as well as for the proposed heat removal system, work is in progress to extend these system codes for the simulation of sCO_2 power cycles [1,4,6–10]. Venker [1] investigated the feasibility of the sCO2-HeRo approach in detail and implemented first extensions in the ATHLET code for the simulation of the heat removal system. Hajek et al. [11] and Vojacek et al. [12] described the basic principles for the integration of the sCO2-HeRo into the European pressurized water reactor fleet including safety, reliability and thermodynamic design considerations. Hofer et al. [9] presented improved models for ATHLET, including heat exchanger and turbomachinery models. The turbomachinery models are performance map based and use a real gas similarity approach to account for changes in the inlet conditions. They also provided a design approach and analysed the sCO_2 cycle with varying decay heat at the maximum ambient temperature [13]. By adapting the rotational speed of the turbomachinery, the cycle is successfully operated in part load. However, in some analysed cases, compressor surge was observed. As part of the project sCO2-4-NPP, the validation status for modelling sCO_2 cycles was provided for the codes CATHARE, Modelica and ATHLET including a blind benchmark [10]. Successful simulations were performed but it was also found that component models need further improvement and some numerical issues need to be solved in the future. Hexemer et. al. [8,14] presented a detailed TRACE model of a recuperated sCO_2 cycle with two turbines. Component modelling, system control, steady state as well as transient results were discussed in detail. They highlighted the importance of performing detailed transient analysis before the system design is finalized. Moreover, attention is drawn to the problem of compressor surge and turbine flow reversal. Nathan [15] investigated control strategies for and the transient behavior of an indirect sCO_2 recompression cycle. The major control strategies are high and low temperature control, turbine bypass, and inventory control. These strategies enable successful cycle operation for different transients, like start-up and shutdown, part-load operation, loss-of-load, loss of heat sink and over-power. Vojacek et al. [16] investigated the control system of the sCO_2 loop at Research Centre Rez experimentally and numerically with Modelica. The parameters of a temperature controller were derived using the Cohen-Coon method. However, it was found that the controller parameters follow the behavior of the specific heat capacity of CO_2 and further manual tuning was inevitable to avoid oscillations.

In this study, the sCO_2 cycle is analysed using ATHLET. First, the preliminary cycle design and layout is presented. Secondly, component modelling and design are discussed briefly, divided into a turbomachinery and heat exchanger section. Thirdly, the control of the compressor inlet parameters via the UHS fan speed is investigated. Fourthly, the start-up of the cycle and different operational readiness states are discussed. Finally, the overall performance of the cycle is analysed highlighting the operational limits.

CYCLE DESIGN AND LAYOUT

In case of an accident, the task of the sCO2-HeRo system is to remove the decay heat reliably over several days. Assuming that other safety systems, as well as electricity supply, is unavailable, the system has to be self-propelling. This means that the power of the turbine must be sufficient to drive the compressor and the fans of the UHS. Moreover, the cycle must be able to remove the residual heat at any expected ambient condition while it decreases exponentially, reducing the power input into the cycle. Therefore, the system must be able to operate over a wide range of conditions. To follow the decay heat curve, the system consists of several units, which are shut down step by step. At the beginning of the accident, the maximum thermal capacity of all systems together can be lower than the initial decay heat, because an inventory loss in the reactor for a limited time span can be tolerated as long as the cooling of the core can be guaranteed [1,13].

This paper deals with the design of one unit of the heat removal system. As a first step, the unit is designed for the highest power input and the highest ambient temperature because this is the design point of the heat exchangers and the highest ambient temperature is the worst-case condition from a thermodynamic point of view. Some conditions in the CO_2 loop can be determined directly from the assumptions summarized in Table 2 in Annex A. These assumptions have been developed in the project sCO2-4-NPP and will be improved continuously. Since the project aims to integrate the sCO2-HeRo system into a pressurized water reactor, the steam side boundary conditions are chosen in accordance with this type of reactor. In a boiling water reactor, the steam pressures and temperatures will be slightly lower due to the lower blow-off pressure. However, in terms of the sCO_2 loop, this has only a minor effect. Therefore, the conclusions from the following analysis are valid for both reactor types. The assumptions in Table 2 are chosen conservatively, e.g. low isentropic turbomachinery efficiencies of 70 % at the design point and moderate temperature differences between the fluids in the heat exchangers are selected.

The remaining conditions in the CO_2 loop are determined through optimization, aiming for the highest excess power ΔP, which is defined as the turbine power reduced by the power consumption of the compressor and the fan. The excess power is maximized because it will decrease with decreasing thermal power input and the system should be able to operate self-propelling as long as possible. The only free parameter to be determined in the optimization procedure is the compressor inlet pressure. All other variables are calculated by basic thermodynamic relations. The optimization process is slightly improved compared to [13] because it also includes the size of the system by specifying its heat removal capacity and the piping pressure losses.

The results of the design process regarding power and mass flow rates are given in Table 3 and the thermodynamic cycle parameters in Table 4, both in Appendix A. The optimization yields an excess power of 283 kW at a relatively high compressor inlet pressure of 126.3 bar. The high operating pressure is a consequence of the need of a high fluid density at the compressor inlet despite the high compressor inlet temperature of 55 °C, which results from the high ambient design temperature of 45 °C.

From Figure 1 it can be observed that the components of the heat removal system are located at different places in the nuclear power plant. Therefore, the length of the connection pipes is assumed to be 22.5 m between each component. The pipe diameters are chosen with regard to density and flow speed to satisfy the specified pressure drop keeping in mind that some additional valves are necessary for the operation and control of the cycle. An inner diameter of 0.1 m was selected for the pipes connected to the compressor and 0.15 m was chosen for the pipes connected to the turbine, considering a pipe roughness of 50 µm. In the current layout, ball valves are included before and after the turbine to be able to disconnect it from the cycle and to avoid reverse flow at unfavourable conditions which might occur during start-up. The bypasses, which are introduced in the following, include a control valve and a check valve with a form loss coefficient of 30 and 6, respectively. They are required for special operating conditions, e.g. for the start-up. In Figure 2, the detailed cycle layout is shown. It includes the bypasses and the controllers discussed in this paper. As mentioned before, the electrical power P_{el} of the turbomachinery (TAC) must be sufficient to power the fans of the UHS. To control the compressor and the turbine inlet condition, the fan speed n_{fan} of the UHS and the shaft speed n_{TAC} can be adapted, respectively. The control of the UHS is discussed and analysed in detail in the following but the control of the turbomachinery is only discussed qualitatively based on the results and will be analysed in more detail in the future. The following bypasses are considered in Figure 2:

- a turbine bypass, connecting turbine inlet and outlet
- a compressor recirculation, connecting compressor outlet and turbine outlet
- and a UHS bypass, connecting turbine outlet and compressor inlet

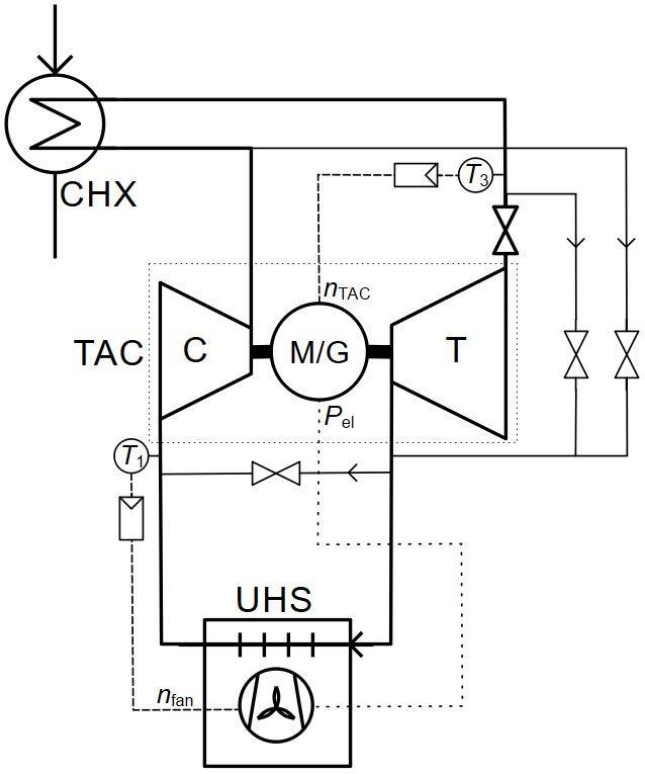

Figure 2: Detailed cycle layout including bypasses and controllers

The turbine bypass and the compressor recirculation are required for start-up and at very low turbomachinery rotational speeds to avoid compressor surge. Possibly only one of these bypasses might be necessary for a future design. The advantage of having the turbine bypass is that it enables fast heat-up of the cycle because the complete mass flow rate flows through the CHX. Furthermore, the turbine bypass can be used to increase the heat removal capacity of the system at full load. A disadvantage is a

higher pressure drop compared to the compressor recirculation. A lower pressure drop is favourable if the current operation point is close to the surge line. The UHS bypass might be required to keep the compressor inlet condition close to its design point at very low ambient temperatures. It enables mixing of hot and cold CO_2, e.g. when the fans of the UHS are switched off or running at minimum speed but the remaining cooling capacity delivers a compressor inlet condition which differs from the desired condition. A modular UHS design, which allows bypassing some UHS modules, is not considered a good alternative because the pressure and temperature in the disconnected modules will decrease considerably compared to the operating conditions of the cycle if the ambient temperature is low. This hampers reconnection of the units to the cycle when the disconnected modules are required again. This might be the case when a running module has to take over the heat removal function from a deliberately or inadvertently stopped module or when the ambient temperature increases again.

TURBOMACHINERY

The performance maps of the sCO_2 turbomachine employed in this study were generated by mean-line analysis codes for compressor and turbine [17]. By specifying the main geometry and inlet conditions of the compressor and turbine, the codes calculate the fluid properties at the inlet and outlet of each component, e.g. the impeller. This is achieved by employing the first law of thermodynamics and the so-called enthalpy loss coefficients. Subsequently, the outlet conditions such as enthalpy and pressure at the outlet of the compressor and turbine are given as the outputs of the codes. Finally, the ratio of total pressures or the specific total isentropic enthalpy difference and the total isentropic efficiencies are calculated.

The mean-line analysis code for the centrifugal compressor was validated with the experimental and numerical results of the project sCO2-HeRo [17]. The code for the radial turbine was validated with the numerical results of the project sCO2-HeRo.

In this study, two preliminary designs, labelled type 1 and type 2, of a sCO_2 centrifugal compressor and radial turbine, which are considered as components of the turbo-alternator-compressor (TAC), are applied to generate performance maps. The design of the compressor was carried out by an in-house code from the chair of turbomachinery (TM) at the University of Duisburg-Essen (UDE), while the experience in the project sCO2-HeRo was taken into account for the design of the turbine. In Figure 3 and Figure 4, two performance maps are shown as an example. All other performance maps and the design parameters are included in Annex B. The presented maps are provided as the input of a recently developed turbomachinery model in ATHLET, which considers real gas effects. Varying inlet conditions are considered by transposing the presented maps to dimensionless maps. The model is based on a real gas similarity approach, which was presented by Pham et al. [18]. The implementation in ATHLET was described in [9].

Figure 3 and Figure 4 display the compressor performance maps of type 1 and type 2 concerning specific total isentropic enthalpy rise over mass flow rate at various rotational speeds. The design point of Type 1 shown in Figure 3 is equal to the design point of the cycle. This design has a small surge margin. As shown in Figure 4, type 2 represents a design with a higher surge margin. The compressor design point of type 2 is still near the surge line but in terms of the cycle design point and during the operation of the cycle a higher margin to the surge line is achieved. Additionally, this provides a good part-load performance. For numerical reasons, the map also includes the instable area left of the surge line.

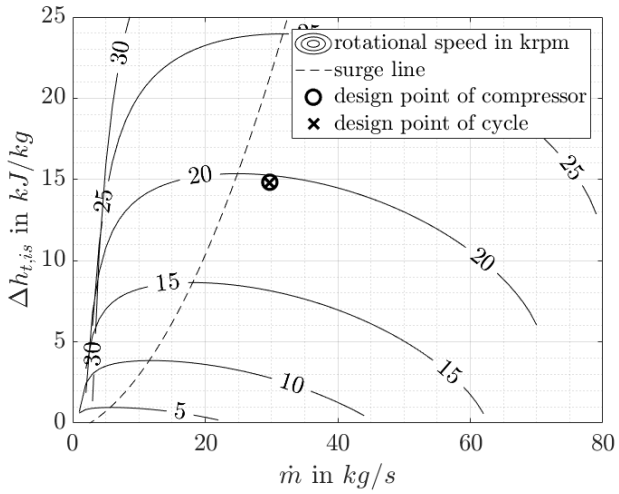

Figure 3: Compressor performance map of type 1 regarding total isentropic enthalpy rise over the mass flow rate

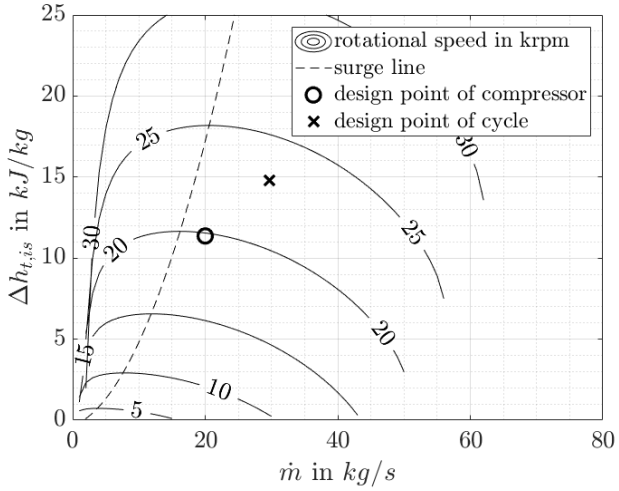

Figure 4: Compressor performance map of type 2 regarding total isentropic enthalpy rise over the mass flow rate

For the cycle design, the isentropic efficiencies of the turbine and compressor were conservatively set to 70 %, as shown in table 1. However, the calculated performance maps yield higher efficiencies around 80 % at the design point of the cycle, although without considering leakage and disk friction. Therefore, to stay in line with the efficiencies specified for the design point of the system and to conservatively account for

further losses, the efficiency of all applied performance maps was multiplied by a factor of 7/8.

HEAT EXCHANGERS

As shown in Figure 1, two heat exchangers are installed in the cycle, the compact heat exchanger (CHX) and the gas cooler, which is also called ultimate heat sink (UHS) in the following. For both heat exchangers, the standard approach of modelling just one representative channel or pipe was applied in ATHLET. The detailed model of the CHX was provided in [19] and the model of the UHS was introduced and validated in [10] and will be extended in this paper. The mentioned reference also includes a detailed description of the experimental UHS, which is scaled up in this paper. The design of both components was derived by scaling of the experimental heat exchanger geometry, which is also given in the mentioned references. Scaling means that the number of channels or pipes and the length is adapted but other geometric relations like the ratio of the heat transfer area on the air-side to the heat transfer area on the CO_2 side are kept constant. The design geometry of the upscaled components is given in Table 5 and Table 6 in Annex A, including the geometry of the heat conduction elements (HCOs), which model the heat conduction in ATHLET.

The upscaled CHX consists of 9000 channels per fluid, which could be arranged into 60 plates per fluid, yielding an approximate heat exchanger size of 1.1 m x 0.5 m x 0.3 m. In accordance with the experimental CHX, form loss coefficients were applied at the CHX inlet and outlet to account for the plenum pressure drop. These coefficients are chosen to match the specified design pressure drop of 2 bar, considering the channel pressure drop which is calculated by ATHLET. This yields 5 for the inlet and 0.5 for the outlet plenum in relation to the pipe flow area. The size of the plate-shaped HCO was adapted to match the thermal resistance of the real configuration and its density was chosen to match the mass of the CHX material.

The UHS consists of 732 pipes on the CO_2-side with an inner diameter of 10 mm and a length of 22 m. The bends of the CO_2 pipes are located outside of the airflow. To consider their fluid volume in the simulation, they were included in the pipe length. In the simulation, the UHS was modelled as a pure counter-current flow heat exchanger where the heat transfer occurs along the whole pipe length. To take the bends into account, the heat transfer area on the CO_2-side, which is the area inside the airflow, was matched by adapting the geometry of a plate-shaped HCO. The air-side is finned, yielding a total heat transfer area of 33000 m² on the air-side. The air-side temperature increase of 25 K was kept constant in the design compared to the experimental heat exchanger, yielding a total air mass flow rate of 382.3 kg/s. The UHS is by far the largest component in the cycle with a total structural mass of 1.81 t. In design conditions, 56.8 % of the total fluid mass of 817 kg is contained in the UHS. Therefore, the UHS represents the largest thermal inertia in the cycle.

The fans of the UHS are installed at the inlet/bottom because high outlet temperatures may occur at low fan speeds or especially when the fans are switched off. Switching the fans off does not reduce the airflow to zero because a natural flow will develop induced by the density difference between the UHS inlet and outlet. To be able to control the UHS also with the fans switched off, it was assumed that this flow can be reduced further, e.g. by flaps at the UHS outlet. At the design point, the power of the fans was calculated by assuming a specific fan power requirement of 8.5 kW_{el}/MW_{th} [20]. In general, the power of the fans can be calculated from the hydraulic power and fan efficiency. The hydraulic power is defined as

$$\Delta P = \Delta p \dot{V} \sim \frac{\dot{m}^2}{0.5(\rho_{in}+\rho_{out})} \frac{\dot{m}}{\rho_{in}} \qquad (1)$$

The pressure drop over the fan Δp is approximately proportional to the mass flow rate squared divided by an average density and the volume flow rate of the fan at the inlet is equal to the mass flow rate divided by the inlet density. Therefore, the power requirement of the fans in off-design conditions can be determined using this proportional relationship together with the design power. This simple approach represents the well-known cubic power dependence of the rotational speed of a pump at a fixed density and enables to calculate the fan power without detailed modelling of the air-side pressure drop.

The heat transfer coefficient on the air-side is determined by a Nusselt correlation, which was also extended and validated for low Reynolds numbers [10]. The relationship between the Reynolds number and the heat transfer coefficient on the air-side for this heat exchanger is exemplarily shown in Figure 5 for an ambient temperature of 45 °C and a wall temperature of 55 °C. At the design point, the heat transfer coefficient on the air-side varies around 28 W/m²K over the length of the UHS. Despite the increased heat transfer area due to the fins, the air-side limits the overall heat transfer.

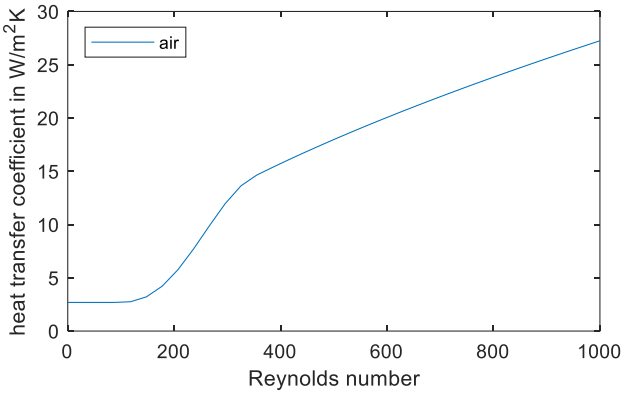

Figure 5: Heat transfer coefficient on the air-side as a function of air Reynolds number

CONTROL OF ULTIMATE HEAT SINK

The outlet condition at the CO_2 side of the UHS must be controlled to keep the compressor inlet in the desired operating range. One option would be to aim for a constant compressor inlet density. Another option is to keep the compressor inlet temperature constant. The advantages of temperature control are technical robustness and simple implementation. Furthermore, a certain temperature difference to the ambient air can be

maintained. This enables a fan operation with a reasonable power requirement. A possible disadvantage of temperature control is that the inlet density changes with pressure. Since no inventory control is considered in the current cycle, the cycle pressures are a function of the current operating condition. Moreover, care must be taken when temperature control is used for sCO_2 because near the pseudocritical point the temperature is almost constant while enthalpy and density are changing rapidly. This effect becomes more pronounced the closer the operational pressure is to the critical pressure of 73.8 bar. For this system, the design operational compressor inlet pressure with 126 bar is considerably above the critical pressure. At the design pressure of 126 bar and the design temperature of 55 °C, the gradient of the density is 14 kg/m³ per Kelvin. Compared to the intended density of about 550 kg/m³ this is assumed to be a moderate gradient. Therefore, temperature control was applied in this analysis. The effect of changing cycle pressure should be analysed later because in the interval from 110 bar to 140 bar, the density at 55°C changes from 415 kg/m³ to 619 kg/m³.

Technically, the speed of the fans should be the variable to be controlled. Due to the lack of a detailed model for the fans, for the simulations, the air mass flow rate was chosen instead as the controlled variable, based on the rationale that the volume flow rate is nearly proportional to the fan speed. Further, controlling the mass flow rate eliminates the influence of the density. The outlet temperature of the UHS is affected by the mass flow rate, inlet pressure and temperature on the CO_2-side. On the air-side, the mass flow rate and the inlet temperature are the relevant parameters. Additionally, wind, humidity and dirt may affect the performance of the UHS but this was not considered. For the determination of the controller parameters, the response of the system to a step function of the CO_2 mass flow rate was considered because this parameter might experience the fastest changes and affects the outlet temperature considerably. In this analysis, a PI-controller was used to control the mass flow rate of the air

$$\dot{m}_{air}(t) = \dot{m}_{air}(t_0) + K_p^* \Delta T(t) + K_i^* \int_{t_0}^{t} \Delta T(\tau) \mathrm{d}\tau. \qquad (2)$$

This can be readily implemented in ATHLET which provides a general model of a PIDT1 controller [21]. Before the controller is started, the air mass flow rate is specified as a function of time. Starting at the time t_0, when the controller is switched on, it varies the air mass flow rate relative to $\dot{m}_{air}(t_0)$. The proportional gain K_p^* and the integral gain K_i^* directly provide the relation between the air mass flow rate in kg/s and the difference of the measured temperature and the set temperature ΔT in K. Therefore, these controller parameters need to be specified with their units.

The controller parameters were determined according to the simple approach of Nathan [15]. First, the proportional gain was selected as high as possible before oscillation occurs. Afterwards, the integral gain was tuned using the selected proportional gain.

The first tuning was conducted at the thermodynamic design conditions of the UHS with the CO_2 mass flow rate decreased to 50 % of its design value. This value was selected because the system must be able to operate in part-load and at lower CO_2 mass flow rates where a changing air mass flow rate has a larger impact. The air mass flow rate required at these conditions is 35 % of its design value. A step increase of 20 % in the CO_2 mass flow rate was applied, resulting in an uncontrolled temperature increase of 5.5 K. Due to the large thermal inertia of the UHS, a new steady outlet temperature is reached after approximately 600 s. The selected proportional gain of 200 kg s^{-1} K^{-1} can reduce the increase to 0.4 K. The tuning of the integral gain is shown in Figure 6. In favour of stability, an integral gain of 5 kg s^{-2} K^{-1} was selected because it is already considerably faster than 2 kg s^{-2} K^{-1} and shows no oscillation at all. This enables stable operation even at lower mass flow rates.

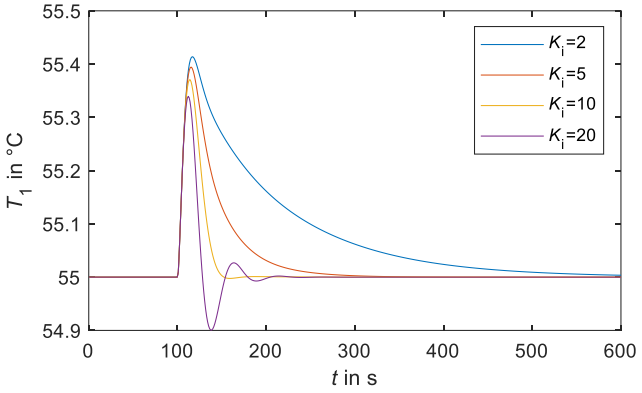

Figure 6: Tuning of the integral gain at the design ambient air temperature of 45 °C

After the tuning at an air temperature of 45 °C, a tuning at –45 °C was conducted because the system should also be able to operate at extreme conditions. The resulting parameters are 20 kg s^{-1} K^{-1} for the proportional gain and 0.2 kg s^{-2} K^{-1} for the integral time constant, respectively. Compared to the previous controller parameters, these parameters differ by a factor of 10, which is reasonable because, at very low ambient temperatures, slight changes in the air mass flow rate have a large impact on the compressor inlet temperature. This is due to the large temperature difference from the CO_2 side to the airside which drives the heat flow. At intermediate ambient temperatures, the controller parameters can be interpolated linearly. In the following chapters, the determined controller parameters are used for the control of the cycle simulations.

STARTUP OF CYCLE

In this chapter, the start of the simulation and different operational readiness states of the system are discussed. It does not cover the start-up from cold shutdown conditions because this is expected to be very challenging at low ambient temperatures. At these temperatures, the CO_2 is in two-phase and liquid conditions and a large part of the fluid accumulates in the UHS and a (fast) start-up of the system might not be possible, e.g. due to material or turbomachinery limitations. Therefore, a new idea is to keep the system in an operational readiness state.

In this paper, an operational readiness state is defined as a state which should enable fast start-up of the system in case of an accident. Moreover, the thermal and electrical energy power consumption of the system must be reasonably low compared to the nuclear power plant. Thus, such a state should fulfil most of the following criteria. First, the compressor inlet condition should already be close to its design point but the rotational speed of the turbomachinery should be low to achieve a reasonable thermal and electrical power consumption. Secondly, a sufficiently high CHX outlet temperature is required to reduce the material stress in the CHX and to be able to start the turbine. Besides, the pressure ratio over the turbine must be high enough to attain forward flow through the turbine when the turbine is connected to the cycle. Thirdly, the throttled steam side limits the thermal power input to the CO_2 cycle. In case of an accident, the valve to the main steam line is opened completely leading to an increased thermal power input to the cycle which in turn allows to increase the speed of the turbomachinery.

The analysis aims to show the general challenges of the start-up and different operational readiness states. To reach this state, the simulation was initialized with a design compressor inlet temperature of 55 °C and a pressure of 101.2 bar resulting from an average density of 335 kg/m³. The air inlet temperature was set to the design temperature of 45°C and the air mass flow rate was set to 3 % of the design flow rate. This should approximately match the conditions with the fans switched off when the UHS is cooled by natural convection [10]. The valves at the turbine inlet and outlet were closed and the turbine bypass was completely open. The compressor recirculation and the UHS bypass were closed in this preliminary analysis.

The procedure shows the start-up and the different operational readiness states step by step. The exact schedule of the different steps needs to be analysed in more detail in interaction with the nuclear power plant. First, the turbomachinery rotational speed is increased to 20 % of the speed occurring at the cycle design point. Secondly, the cycle is heated up with a small amount of steam. Thirdly, the controller of the compressor inlet temperature is switched on with a set point of 55 °C. Fourthly, the opening of the turbine bypass is decreased to decrease the compressor mass flow rate and increase the pressure ratio and the CHX outlet temperature. This state is considered as the first operational readiness state (ORS1). The only difference to the next one (ORS2) is that the turbine bypass valve is throttled further, which yields a further increase of the pressure ratio and the CHX outlet temperature. To reach the last operational readiness state (ORS3), discussed here, the valves at the turbine are opened and the turbine bypass valve is closed completely. From this point, the thermal power of the CHX and the speed of the turbomachinery can be increased rapidly to design operation conditions. This represents the initial point of the cycle performance analysis in the next chapter. In Table 1 the conditions of the three operational readiness states are summarized for type 2 turbomachinery. This type is preferred due to the higher surge margin. The results in Table 1 are preliminary because the operating points are located far from the design point, where the accuracy of the models and the input needs to be analysed further. Moreover, the guess for the turbomachinery speed and the steam mass flow rate, which determines the thermal power of the CHX, might be adapted, e.g. to further reduce the thermal power consumption. Taking this into account, it can be observed from the total power of the system that it might be possible to achieve a self-propelling operational readiness state (ORS3) at only 12 % of the design thermal power input. Additionally, the other two operational readiness states show a low required power at similar operating conditions. For all three states, the compressor inlet pressure is already close to its design point. Furthermore, a CHX outlet temperature of approximately 150 °C seems to be sufficient to start the turbine at these conditions. ORS 1 yields the highest surge margin due to the larger opening of the turbine bypass but shows the highest power consumption and the lowest CHX outlet temperature. ORS 2 and ORS 3 are very similar except for the turbine operating in ORS 3. Therefore, ORS 3 will be preferred if the self-propelling operation is confirmed in the future.

Table 1: Conditions for the operational readiness states (ORS) of the system with type 2 turbomachinery

	Unit	ORS1	ORS2	ORS3
Turbomachinery speed relative to the cycle design point	%	20	20	20
Turbine bypass valve	%	58	24	0
Turbine valves	%	0	0	100
Compressor inlet p	bar	117.3	122.1	122.6
Compressor outlet p	bar	119.4	125.2	125.7
CHX outlet T	°C	111	150	155
CHX thermal power	MW	1.2	1.2	1.2
Mass flow rate (CO_2)	kg/s	8.5	5.9	5.7
Compressor efficiency	%	50.7	68.2	68.9
Turbine efficiency	%	0	0	71.4
Compressor power	kW	7.1	5.0	4.9
Turbine power	kW	0	0	6.5
Fan power	kW	0.6	0.4	0.4
Total power	kW	-7.7	-5.4	1.2

In the following, the challenges of the start-up are discussed. If the cycle is heated too fast, the rapidly expanding fluid in the CHX might build up pressure quickly, forcing the compressor to surge due to decreasing mass flow. Additionally, the control of the compressor inlet temperature needs to be switched on soon enough to avoid a density drop at the compressor inlet. Depending on the characteristic of the turbine bypass valve, the valve opening must be reduced considerably. In this analysis, the non-linear characteristic observed in [10] is assumed. At small openings, a further throttling must be done carefully to avoid compressor surge. Before the valves at the turbine are opened, it must be ensured that the current conditions will result in a forward flow over the turbine, e.g. pressure ratio must be high enough. Otherwise, no flow or even reverse flow may occur.

With the current model, this could be observed by a decreased time step and an infinite iteration in the search of an adequate mass flow balance between the bypass and the turbine.

CYCLE PERFORMANCE ANALYSIS

In this chapter, the cycle is analysed over a wide range of conditions to show the operational limits of the cycle. All analysed operation points were approached via transient ramps in the turbomachinery rotational speed and the steam mass flow rate, while the compressor inlet temperature T_1 was held constant by the controller and the steam inlet temperature was equal to its design value in Table 2. Then all boundary conditions were kept constant until a steady-state was reached. A change of less than 0.5 % in terms of the excess power output ΔP can be reached for all investigated cases. Most cases are considerably closer to a real steady-state with deviations of less than 0.1 %. The highest deviations occur at an ambient temperature of -45 °C and are discussed below. Additionally, it should be mentioned that the following figures are based on the conservative assumptions made in the design chapter. Less conservative assumptions, like higher turbomachinery efficiencies especially in part-load, will improve the performance of the system.

Figure 7 shows the excess power output ΔP of the cycle using type 2 performance maps at the design conditions, namely at a compressor inlet temperature of 55 °C and an air inlet temperature of 45 °C. In terms of the power of the CHX $\dot{Q}_{CHX}$ and turbomachinery rotational speed n, the cycle design point is located at 10 MW and 23 krpm, respectively. The turbomachinery rotational speed and the steam mass flow rate are varied from 20 % to 120 % compared to their value at the design point of the cycle. The colourmap indicates that the excess power is decreasing both with decreasing $\dot{Q}_{CHX}$ and decreasing n. Moreover, Figure 7 shows regions in white where the cycle cannot be operated. First, in the lower right, the operation range is limited by the heat transfer in the CHX and the maximum steam temperature. Thermodynamically, the turbine inlet temperature T_3 is always lower than the maximum steam temperature. The maximum steam temperature results from the maximum operating pressure of the reactor in case of a BWR; for PWR it is determined by secondary pressure or the average primary coolant temperature in case of exposed steam generator tubes. The overheating, resulting from the latter case is assumed in Table 2 in Annex A. Secondly, in the upper left, the operation range is limited because the excess power output drops below zero, which means that the cycle is not self-propelling any more.

In Figure 7, it can be observed that ΔP decreases with decreasing $\dot{Q}_{CHX}$ and n and an operation line in terms of maximum ΔP exists between the two borders. From a Carnot point of view, operation at the highest turbine inlet temperature should yield the highest efficiency. This operation line, which is equal to the right border of the operation range, is feasible because ΔP is higher than zero. Moreover, the compressor inlet pressure increases to about 135 bar with decreasing n along this line. This is a result of the decreasing density on the high-pressure side. However, the highest ΔP does not occur at the highest turbine inlet temperature. This is mainly due to the turbine and compressor efficiencies departing from their optimal value. Over the whole speed range, the highest turbine efficiencies are reached for conditions where the turbine inlet density is close to its design inlet density. Therefore, another operation strategy would be to keep the inlet density of the turbine constant instead of the inlet temperature. Indirectly this also ensures relatively constant compressor inlet densities because both densities in the cycle are linked to each other as long as no CO_2 mass is removed or added. To keep the turbine inlet density constant, the turbine inlet temperature must be decreased with decreasing turbomachinery rotational speed because the pressure ratio and the turbine inlet pressure are also decreasing. However, it should be mentioned that the goal of the system is to reliably remove the decay heat and not to maximize its power output. Therefore, it needs to be analysed in the reactor simulations which strategy enables a more reliable operation in interaction with the nuclear power plant.

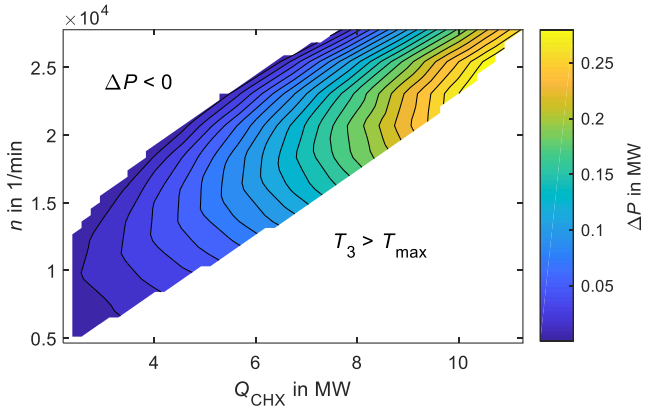

Figure 7: Excess power output of the cycle at $\boldsymbol{T_1 = 55}$ °C and $\boldsymbol{T_{air,in} = 45}$ °C with type 2 turbomachinery

Compared to the type 2 turbomachinery, operation with type 1 turbomachinery yielded slightly higher ΔP mainly because the compressor efficiency of type 1 is slightly higher. Regarding compressor efficiency, the highest difference is 2.9 % and occurs at the design point of the cycle because type 2 turbomachinery is designed for part-load operation with a higher compressor surge margin, as mentioned in the turbomachinery chapter. From the design point of the cycle, the resulting ΔP difference of 35 kW continuously decreases with decreasing speed. At the lowest speeds, the type 1 turbomachinery almost reaches the surge line. Therefore, care must be taken when this type of turbomachinery is applied, e.g. the compressor recirculation valve must be opened slightly to increase the surge margin. However, this might decrease the excess power to zero, resulting in a stop of the system. Furthermore, the higher surge margin of type 2 is an advantage during start-up. Due to these reasons, type 2 turbomachinery is preferred.

Figure 8 shows the excess power output ΔP of the cycle using type 2 performance maps at the off-design conditions, namely at a compressor inlet temperature of 35 °C and an air

inlet temperature of 25 °C. For $\dot{Q}_{CHX}$ and n the same range is shown as in Figure 7. At these conditions, different behaviour of ΔP can be observed. First, the area where ΔP is smaller than zero increases except for low $\dot{Q}_{CHX}$. Secondly, the maximum of ΔP is located at a lower $\dot{Q}_{CHX}$ and n. Thirdly, the lower limit of the cycle performance map is slightly shifted to lower n, especially for higher $\dot{Q}_{CHX}$. The first two observations are mainly due to an increasing fan power. The required fan power increases significantly, especially at high $\dot{Q}_{CHX}$ and n, because the required air mass flow rate considerably increases compared to the design airflow rate of the UHS and the required power increases cubically with air mass flow rate. The reason for the considerably higher demand of air mass flow rate is that the major part of the heat has to be removed at the pseudocritical temperature of CO_2 at a lower system pressure and in this case, this significantly decreases the available temperature difference between the CO_2 and the air. Additionally, the increased heat transfer coefficient on the CO_2-side hardly influences the overall heat transfer coefficient because the air-side limits the heat transfer. The third observation, the shift of the lower limit, results from the higher available enthalpy difference in the cycle. To reach the same $\dot{Q}_{CHX}$, a lower cycle mass flow rate is required and, therefore, a lower n compared to the previous case.

For these operation conditions, many operation points with the type 1 turbomachinery would be close to or beyond the surge line. This is because decreasing the compressor inlet temperature generally shifts the cycle operation closer to the surge line. Furthermore, controlling the compressor inlet temperature at pressures and temperatures closer to the critical point is probably inappropriate, as mentioned in the control chapter.

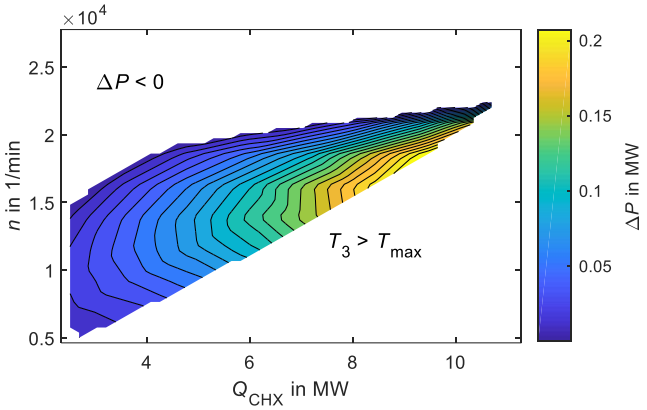

Figure 8: Excess power output of the cycle at $\boldsymbol{T_1 = 35}$ °C and $\boldsymbol{T_{air,in} = 25}$ °C with type 2 turbomachinery

After discussing these issues, the question arises how the cycle can be operated reliably over the whole range of ambient temperatures, e.g. from -45 °C to 45 °C. Since no inventory control is considered, a decreasing compressor inlet temperature also results in decreasing cycle pressure. Therefore, not only the performance changes significantly at lower compressor inlet temperatures but also the operation conditions might drop into the two-phase region. An easy approach to avoid all these issues would be to keep the compressor inlet temperature constant over the whole range of ambient temperatures. As an example, the cycle performance at an ambient temperature of -45 °C with the compressor inlet kept constant at 55 °C is shown in Figure 9. At low ambient temperatures the cycle performance map qualitatively still equals the performance shown in Figure 7. The main difference is a generally higher ΔP resulting from a lower fan power because the fan speed of the UHS must be decreased to keep the compressor inlet temperature constant. For the operation of the cycle the same approaches, which were described for an ambient temperature of 45 °C, are valid. However, for very low ambient temperatures it might not be sufficient to only decrease the fan speed because the expected heat removal by natural convection would be too high. Thus, either the natural convection airflow must be throttled further, e.g. by flaps at the UHS outlet, or a part of the CO_2 flow must bypass the UHS to reach a constant compressor inlet temperature by mixing cold and hot CO_2. Moreover, it can be observed that the controller parameters need further tuning at very low air mass flow rates due to the non-linear behaviour of the heat transfer coefficient shown in Figure 5.

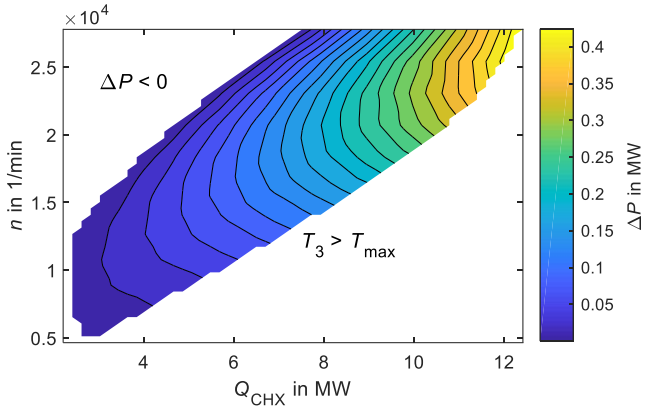

Figure 9: Excess power output of the cycle at $\boldsymbol{T_1 = 55}$ °C and $\boldsymbol{T_{air,in} = -45}$ °C with type 2 turbomachinery

As shown in Figure 7 and Table 3, the excess power at the design point is 283 kW. Since only a self-propelling system is required, the turbine power can be decreased. Therefore, it is an option to open the turbine bypass slightly to decrease the mass flow rate over the turbine and increase the mass flow rate in the cycle, resulting in higher heat removal from the nuclear power plant. However, the valve has to be operated at a very small opening. With the current valve design, the opening must be lower than 3.9 % to keep the system self-propelling. This opening increases the cycle mass flow rate by 6.3 kg/s and the thermal power of the CHX by 2.2 MW. For better control in this operation mode, a second turbine bypass with a smaller pipe diameter would be advantageous.

CONCLUSIONS

In this study, the sCO_2 heat removal system was designed and simulated under varying ambient and steam side boundary conditions, using the assumptions developed in the project sCO2-4-NPP. Bypasses were considered in the layout of the

cycle to cope with special operation conditions, e.g. start-up. Since cold start-up at very low ambient temperatures is challenging, it was proposed to start the system from an operational readiness state. In this state, the turbomachinery and the fans are already under operation at low speeds and the compressor inlet condition is close to its design point. This enables fast start-up of the system in case of an accident in the nuclear power plant. At 20 % turbomachinery rotational speed compared to the design point of the cycle, a self-propelling system could be achieved at 12 % of the design thermal power.

To operate the system under changing ambient conditions, the compressor inlet condition needs to be controlled. Compressor inlet temperature control was selected because the cycle operation pressure was sufficiently higher than the critical pressure of CO_2. A PI-controller was used to change the mass flow rate of the fans. For low ambient temperatures, adapted controller parameters are required due to the higher sensitivity of the compressor inlet temperature to the air mass flow rate. Therefore, variable controller parameters which depend on ambient temperature are suggested. In the simulation, the controller was operated successfully over a wide range of conditions. However, the performance and the control of the UHS and the system at very low ambient temperatures with fans switched off should be analysed in more detail. If the UHS outlet condition cannot be controlled reliably, a UHS bypass could be used to mix hot and cold CO_2 to keep the compressor inlet at the desired condition.

The performance analysis of the system suggests that it is a good option to operate the system at the design compressor inlet temperature of 55 °C at any ambient or steam-side boundary condition. It is not preferred to operate the system closer to the critical point of CO_2 because this introduces further operational challenges. Due to higher isentropic efficiency, type 1 turbomachinery provides a higher excess power. However, type 2 turbomachinery is preferred due to the higher surge margin because only a self-propelling and reliable system operation is required. With decreasing thermal power of the CHX, the turbomachinery rotational speed must be decreased to keep the system self-propelling. Different operation strategies are feasible and need to be tested in interaction with the nuclear power plant. Keeping the turbine inlet density constant results in a higher excess power than constant turbine inlet temperature. A good start for the reactor simulations might be to keep the turbine inlet temperature constant at its design point because this should also balance the heat removal from the reactor when the decay power is lower than the heat removal capacity of the systems. At a higher decay power, the system should be operated at the maximum allowable speed to maximize the heat removal and keep the inventory loss of the reactor to a minimum. At these conditions, it might be possible to increase the heat removal further by opening the turbine bypass slightly.

The conclusions drawn in this work are valid for the sCO2-HeRo system in general and are independent of the type of reactor. However, the next step is to simulate the heat removal system in interaction with the nuclear power plant because the thermal-hydraulic behaviour and the limitations depend on the reactor type. An integrated analysis enables testing and further improvement of the operational strategies provided in this paper.

NOMENCLATURE

$\Delta h_{is,t}$	specific total isentropic enthalpy difference (J/kg)
$\dot{m}$	mass flow rate (kg/s)
n	rotational speed (1/min)
p	pressure (bar)
T	temperature (°C)
ΔP	excess power (MW)
$\dot{Q}$	thermal power (MW)

Subscripts

1	compressor inlet
3	turbine inlet
el	electrical

Acronyms

CHX	compact heat exchanger
HeRo	heat removal system
ORS	operational readiness state
sCO_2	supercritical carbon dioxide
TAC	turbomachinery (turbo-alternator-compressor)
UHS	ultimate heat sink

ACKNOWLEDGEMENTS

The research presented in this paper has received funding from the Euratom research and training programme 2014-2018 under grant agreement No. 847606 “Innovative sCO2-based Heat removal Technology for an Increased Level of Safety of Nuclear Power plants” (sCO2-4-NPP).

The work of University of Stuttgart was also funded by the German Ministry for Economic Affairs and Energy (BMWi. Project No. 1501557) on basis of a decision by the German Bundestag.

REFERENCES

[1] Venker, J. (2015) Development and Validation of Models for Simulation of Supercritical Carbon Dioxide Brayton Cycles and Application to Self-Propelling Heat Removal Systems in Boiling Water Reactors. Stuttgart. https://doi.org/10.18419/opus-2364

[2] sCO2-HeRo. http://www.sco2-hero.eu/

[3] Benra, F.K., Brillert, D., Frybort, O., Hajer, P., Rohde, M., Schuster, S. et al. (2016) A supercritical CO2 low temperature Brayton-cycle for residual heat removal. *The 5th International Symposium-Supercritical CO2 Power Cycles*, 1–5. https://doi.org/10.1007/s13398-014-0173-7.2

[4] Wu, P., Gao, C. and Shan, J. (2018) Development and Verification of a Transient Analysis Tool for Reactor System Using Supercritical CO_2 Brayton Cycle as Power Conversion System. *Science and Technology of Nuclear Installations*, Hindawi. 2018, 1–14.

https://doi.org/10.1155/2018/6801736
[5] Bestion, D. (2008) System code models and capabilities. *THICKET*, Grenoble. p. 81–106.
[6] Mauger, G., Tauveron, N., Bentivoglio, F. and Ruby, A. (2019) On the dynamic modeling of Brayton cycle power conversion systems with the CATHARE-3 code. *Energy*, Elsevier Ltd. 168, 1002–16. https://doi.org/10.1016/j.energy.2018.11.063
[7] Batet, L., Alvarez-Fernandez, J.M., Mas de les Valls, E., Martinez-Quiroga, V., Perez, M., Reventos, F. et al. (2014) Modelling of a supercritical CO_2 power cycle for nuclear fusion reactors using RELAP5–3D. *Fusion Engineering and Design*, North-Holland. 89, 354–9. https://doi.org/10.1016/J.FUSENGDES.2014.03.018
[8] Hexemer, M. (2011) Supercritical CO_2 Brayton Cycle Integrated System Test (IST) TRACE Model and Control System Design. *Supercritical CO2 Power Cycle Symposium*, 1–58.
[9] Hofer, M., Buck, M. and Starflinger, J. (2019) ATHLET extensions for the simulation of supercritical carbon dioxide driven power cycles. *Kerntechnik*, 84, 390–6. https://doi.org/10.3139/124.190075
[10] Hofer, M., Buck, M., Cagnac, A., Prusek, T., Sobecki, N., Vlcek, P. et al. (2020) Deliverable 1.2: Report on the validation status of codes and models for simulation of sCO2-HeRo loop. sCO2-4-NPP.
[11] Hajek, P., Vojacek, A. and Hakl, V. (2018) Supercritical CO_2 Heat Removal System - Integration into the European PWR fleet. *2nd European SCO2 Conference*, Essen. p. 0–7. https://doi.org/10.17185/duepublico/460
[12] Vojacek, A., Hakl, V., Hajek, P., Havlin, J. and Zdenek, H. (2016) Deliverable 1.3: Documentation system integration into European PWR fleet. sCO2-HeRo.
[13] Hofer, M., Buck, M. and Starflinger, J. (2021) Operational analysis of a self-propelling heat removal system using supercritical CO2 with ATHLET. *4th European Supercritical CO2 Conference*, Prague.
[14] Hexemer, M.J., Hoang, H.T., Rahner, K.D., Siebert, B.W. and Wahl, G.D. (2009) Integrated Systems Test (IST) Brayton Loop Transient Model Description and Initial Results. *S-CO2 Power Cycle Symposium*, Troy. p. 1–172.
[15] Carstens and Nathan. (2007) Control strategies for supercritical carbon dioxide power conversion systems. *Massachusetts Institute of Technology*,.
[16] Vojacek, A., Melichar, T., Hajek, P., Doubek, F. and Hoppe, T. (2019) Experimental investigations and simulations of the control system in supercritical CO2 loop. *3rd European Conference on Supercritical CO2 (SCO2) Power Systems*,. https://doi.org/10.17185/duepublico/48916
[17] Ren, H., Hacks, A., Schuster, S. and Brillert, D. (2021) Mean-line analysis for supercritical CO_2 centrifugal compressors by using enthalpy loss coefficients. *4th European Supercritical CO2 Conference*, Prague.
[18] Pham, H.S., Alpy, N., Ferrasse, J.H., Boutin, O., Tothill, M., Quenaut, J. et al. (2016) An approach for establishing the performance maps of the sc-CO2 compressor: Development and qualification by means of CFD simulations. *International Journal of Heat and Fluid Flow*, 61, 379–94. https://doi.org/10.1016/j.ijheatfluidflow.2016.05.017
[19] Hofer, M., Buck, M., Strätz, M. and Starflinger, J. (2019) Investigation of a correlation based model for sCO2 compact heat exchangers. *3rd European Supercritical CO2 Conference*, Paris. p. 1–9. https://doi.org/10.17185/duepublico/48874
[20] Alfani, D., Astolfi, M., Binotti, M., Silva, P. and Macchi, E. Off-design Performance of CSP Plant Based on Supercritical CO2 Cycles. *SOLARPACES 2019: International Conference on Concentrating Solar Power and Chemical Energy Systems*,.
[21] Austregesilo, H., Bals, C., Hora, A., Lerchl, G., Romstedt, P., Schöffel, P. et al. (2016) ATHLET Models and Methods. Garching.

ANNEX A: CYCLE AND HEAT EXCHANGER DESIGN

In Table 2 the assumptions for the cycle design are given and in Table 4 and Table 3 the results of the cycle design are provided. Table 5 and Table 6 show the CHX and UHS design, respectively.

Table 2: Assumptions for the cycle design

Name	Value	Unit
Thermal power of one unit	10	MW
Steam pressure	82	bar
Steam inlet temperature	308	°C
Turbine inlet temperature	286.6	°C
Compressor inlet temperature	55	°C
Ambient temperature	45	°C
Pressure drop of CHX (CO_2)	2	bar
Pressure drop of UHS (CO_2)	0.25	bar
Piping pressure drop (CO_2)	2	bar
Pressure ratio of the compressor	1.7	
Isentropic efficiency of the compressor	0.7	
Isentropic efficiency of the turbine	0.7	
Specific power of fans [20]	8.5	kW_{el}/ MW_{th}

Table 3: Results of the cycle design

Name	Value	Unit
Thermal power of CHX	10.0	MW
Thermal power of UHS	9.6	MW
Compressor power	630	kW
Turbine power	994	kW
Fan power	82	kW
Excess Power	283	kW
CO_2 mass flow rate	29.7	kg/s
steam mass flow rate (with $T_{H2O,out} = 150$ °C)	4.6	kg/s
Air mass flow rate (with $T_{air,out} = 70$ °C)	382.3	kg/s

Table 4: Thermodynamic results of the cycle design

	p [bar]	T [°C]
Compressor inlet	126.3	55.0
Compressor outlet	214.7	80.8
CHX inlet	214.2	80.8
CHX outlet	212.2	286.6
Turbine inlet	211.7	286.6
Turbine outlet	127.5	243.2
UHS inlet	127.0	243.2
UHS outlet	126.8	55.0

Table 5: CHX design

Name	Value	Unit
Number of channels per side	9000	
Channel geometry	2x1	mm²
Channel length	1.1	m
HCO total length (equal to channel length)	1.1	m
HCO width (equal to channel perimeter)	6	mm
HCO effective thickness	1.53	mm
Steel mass	972	kg

Table 6: UHS design

Name	Value	Unit
Number of pipes (CO_2)	732	
Pipe diameter	10	mm
Pipe length	22	m
Total airflow area in UHS	240	m²
Total heat transfer area (air)	33000	m²
HCO total length (equal to pipe length)	22	m
HCO width (artificial to account for pipe section outside of the airflow)	27.5	mm
HCO effective thickness	1	mm
Total steel/aluminium mass	1.81	t

ANNEX B: PERFORMANCE OF TURBOMACHINE

The design parameters of type 1 and type 2 applied in this paper are displayed below.

Table 7: Design parameters of turbomachinery

	Parameter	Type 1	Type 2	Unit
Compressor	Inlet total pressure	126.3	126.3	bar
	Inlet total temperature	328.15	328.15	K
	Total pressure ratio	1.7	1.53	–
	Mass flow rate	29.7	20	kg/s
	Rotational speed	19728	19847	rpm
Turbine	Inlet total pressure	211.7	211.7	bar
	Inlet total temperature	559.72	559.72	K
	Total pressure ratio	1.66	1.66	–
	Mass flow rate	29.7	29.7	kg/s
	Rotational speed	19728	23139	rpm

The other performance maps of the applied turbomachines are displayed below:

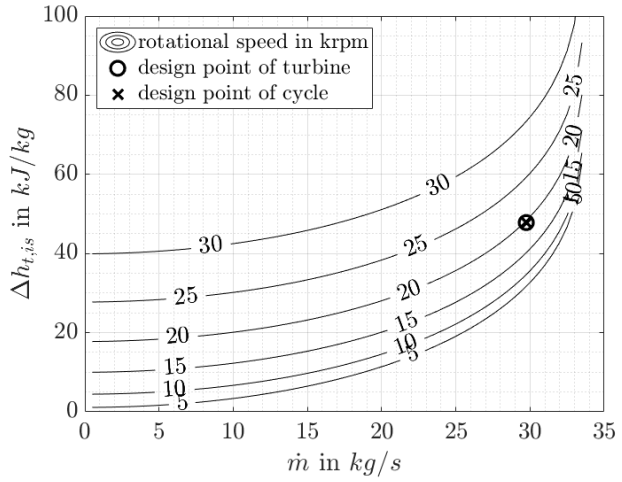

Figure 10: Turbine performance map of type 1 regarding total isentropic enthalpy drop over the mass flow rate

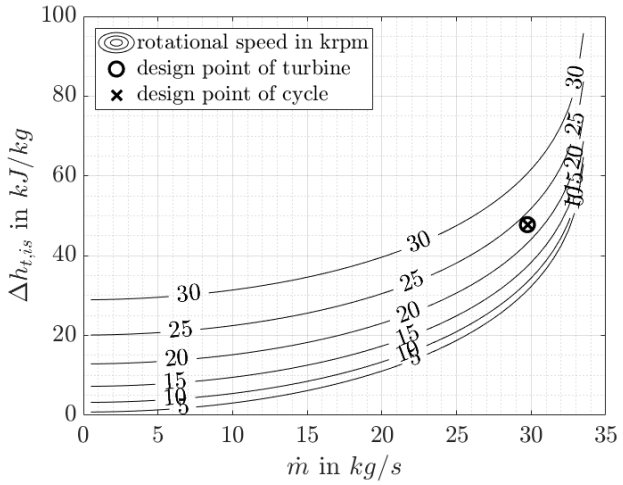

Figure 11: Turbine performance map of type 2 regarding total isentropic enthalpy drop over the mass flow rate

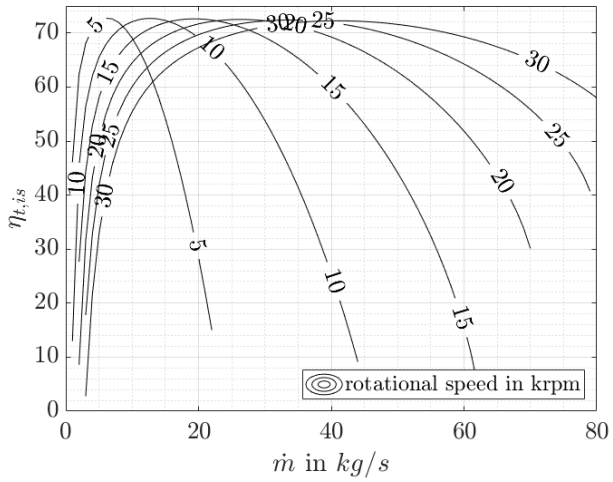

Figure 12: Compressor performance map of type 1 regarding total isentropic efficiency over the mass flow rate

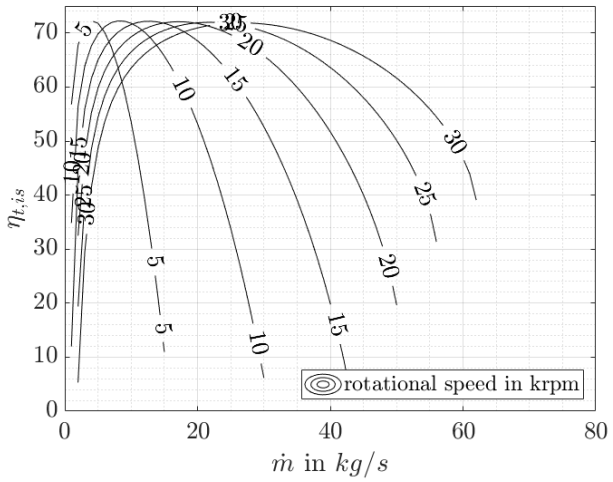

Figure 13: Compressor performance map of type 2 regarding total isentropic efficiency over the mass flow rate

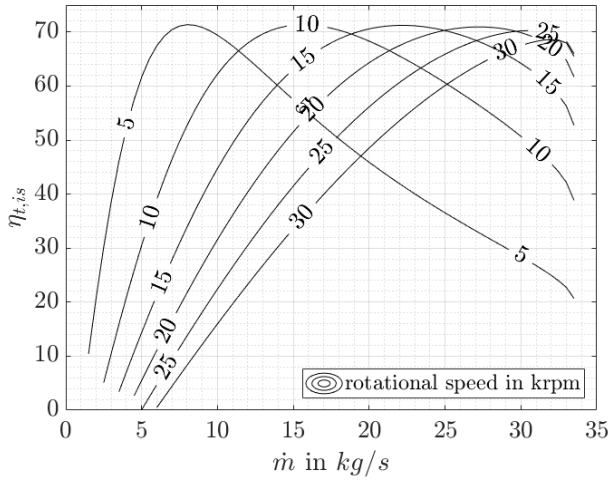

Figure 14: Turbine performance map of type 1 regarding total isentropic efficiency over the mass flow rate

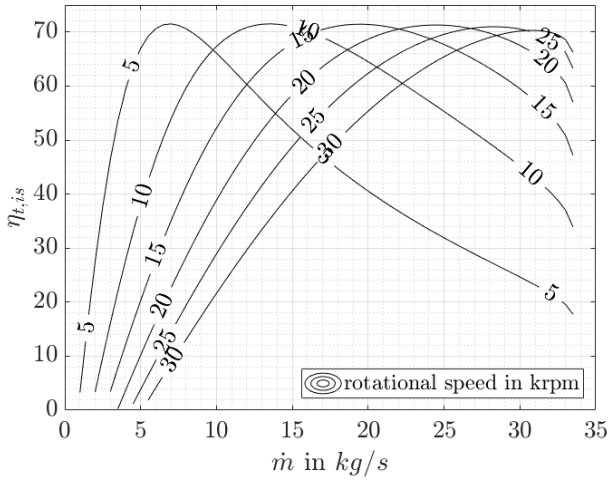

Figure 15: Turbine performance map of type 2 regarding total isentropic efficiency over the mass flow rate

DOI: 10.17185/duepublico/73943
URN: urn:nbn:de:hbz:464-20210330-090812-4